

Spectroscopic atlas of H α and H β in a sample of northern Be stars[★]

G. Catanzaro^{★★}

INAF-Catania Astrophysical Observatory, via S. Sofia 78, I-95123, Catania, Italy
e-mail: giovanni.catanzaro@oact.inaf.it

Received 10 September 2012 / Accepted 7 December 2012

ABSTRACT

Context. Be stars are fast-rotating early-type emission line stars. It is generally assumed that observed emission is generated in a rotating disk-like envelope, as supported by the observed correlation between the stellar projected rotational velocity $v \sin i$ and the width of the emission lines. Then, high-resolution spectroscopic observations of Balmer lines profiles play an important role in putting constraints on Be stars modeling.

Aims. We present Balmer lines spectroscopy for a sample of 48 Be stars. For most of them, H α and H β have been observed more than two times, in a total period spanning almost two years between 2008 and 2009.

Methods. Spectral synthesis of the H α profile was performed following two steps: photospheric contribution was computed by using Kurucz's code ATLAS9 and SYNTHE, and disk emission was derived by the approach of Hummel & Vrancken (2000, A&A, 302, 751).

Results. For 26 out of 48 stars, a modeling of the total H α emission, i.e. photospheric absorption plus disk net emission, has been attempted. By this modeling we derived an estimation of the disk radius, as well as the inclination angle between the rotational axis with line of sight and the base density at the stellar equator. For the stars observed more than once, we also discuss the variability of H α and H β for what concerns both the equivalent width and the spectral profile. We found 16 stars with variable equivalent width and 7 stars with clear signs of profile variations.

Conclusions. For all the stars in our sample, we derive all the fundamental astrophysical quantities, such as, effective temperature, gravity, and projected rotational velocity. We found 13 stars whose equivalent width is variable with a confidence level greater than 80% and 7 object for which spectral profiles show change with time. According to the commonly used classification scheme, we classified 16 stars as belonging to class 1, 13 to class 2, 11 are shell stars, 6 objects do not show net emission, and 2 stars display transitions from class 1 and 2. For the class 1 stars, we confirm the correlation between $v \sin i$ and peak separation. Concerning the geometry of the disk, we derived the base density at the stellar equator, the radius, and the inclination angle between rotational axis and line of sight. The maximum concentration of stars occurs for disk dimensions ranging in the interval of 6 to 8 stellar radii and for inclination angles going from 23° to 35°.

Key words. Stars: emission-line, Be – stars: fundamental parameters

1. Introduction

Classical Be stars are early-type B-type stars whose spectra have one or more emission lines in the Balmer series. In particular, the H α emission line is typically the dominant feature in the spectra of such stars, and many authors have modeled H α line profiles to understand the Be star phenomenon better.

The emission lines observed in the spectra are explained in terms of the recombination that occurs in a flattened circumstellar disk, according to the widely accepted model first proposed by Struve (1931). The disk is a decretion disk; i.e., the source of the disk material is the central star, generated by the equatorial flow of stellar material. One of the key factors in creating the disk is supposed to be the very high value of rotational velocity. In fact, Be stars are known to have higher rotational velocities than a sample of normal B-type stars. From statistical considerations on the $v \sin i$ distribution among Be stars, Porter (1996)

estimated that Be stars rotate at a equatorial velocity equal to 80 % of the critical rotation velocity:

$$v_{\text{eq}} = 0.8 \sqrt{\frac{GM_*}{R_*}}.$$

The observed emission lines take a variety of shapes, which following the scheme proposed by Hanuschik (1996), range from wine bottle profiles, singly or double-peaked profiles, to shell spectra, when the central absorption must extend below the stellar continuum flux. The various shapes are explained as a dependency of i , the inclination angle of the star's rotation axis to the observer's line of sight. In particular, shell profiles occur only when the disk is viewed equator-on ($i = 90^\circ$), while the single peak and wine bottle occur only for near pole-on ($i = 0^\circ$) viewings, and double-peaked profiles occur at mid-inclination angles.

Double-peaked profiles have been observed both symmetric, which are the two peaks have the same intensity, and asymmetric, the peaks have different height over the continuum level. The current theory is that asymmetry arises from one-armed density waves in the circumstellar disk, which is also known as the global disk oscillation model. In this model, a one-armed oscillation mode is superposed on an unperturbed, axisymmetric disk (Okazaki, 1997). Another aspect of Be stars emission

[★] Table B.1 and all observed spectra are available in electronic form at the CDS via anonymous ftp to cdsarc.u-strasbg.fr (130.79.128.5) or via <http://cdsweb.u-strasbg.fr/cgi-bin/qcat?J/A+A/>

^{★★} I wish to dedicate this paper to my child never born, to keep track of his passage through my life.

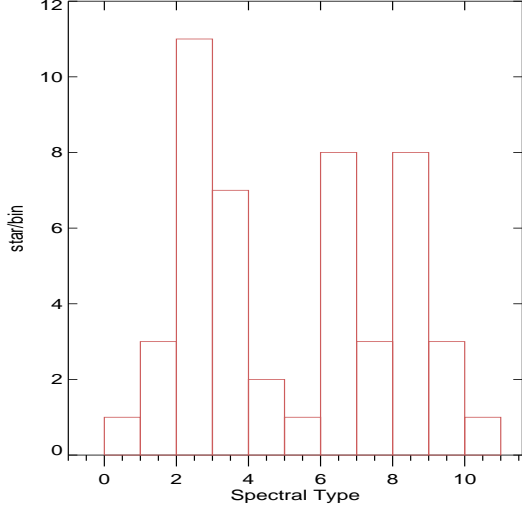


Fig. 1. Histogram showing the distribution of program stars as a function of spectral type.

is their variability. For example, about one third of all double-peaked profiles exhibit changing asymmetry, with the so-called violet-to-red ratio (V/R) being cyclically variable on timescales of years to decades.

Observations in different spectral regions help astronomers probe different regions of the stellar disk and then put constraints on modeling these stars. For example, recently Meilland et al. (2007) have used VLTI/AMBER to observe α Arae in the Br γ line, which was constrained very strongly the rotational property of its disk, concluded that its rotation is purely Keplerian.

In this paper we present an atlas of observed H α and H β spectral lines in a sample of bright Be stars. We payed particular attention to modeling the H α profile and to the time variability of Balmer lines profiles.

2. Observation and data reduction

The idea that underlies this catalog is to create a homogeneous data set of stars observed with the same instrument, the telescope of the *M.G. Fracastoro* station of INAF-Catania Astrophysical Observatory. For this purpose, we queried the “Catalogue of Be stars” compiled by Jaschek & Egret (1982) selecting all the objects with $V \leq 7$ and observable at the latitude of the observatory, which means all the stars with $\delta \geq -22^\circ$. The result of this query is the sample of 48 Be stars reported in Table 1. The limiting magnitude was chosen to obtain a good compromise between the exposure time and the signal-to-noise ratio.

The present catalog is based on new spectroscopic observations of all the stars in our sample, which spectral type are distributed between B1 and A0 (according to the histograms displayed in Fig. 1), and luminosities classes are III, IV, and V, as in the SIMBAD database¹. Some of these stars’ spectra have never been published in other catalogs similar to ours, at least to our knowledge.

All the spectra of our program stars have been acquired with the 91-cm telescope and FRESCO, the fiber-fed REOSC echelle spectrograph that allows spectra to be obtained in the

Table 1. Spectral types, luminosity classes, Strömgren photometry, and derived effective temperatures for our program stars. Spectral types and luminosity classes are taken from the SIMBAD database

HD	Spec.	b-y	m ₁	c ₁	H β	T _{eff} (K)
6811	B7 Ve	0.006	0.082	0.697	2.676	12600
10516	B2 Vep	—	—	—	—	25410
11415	B3 III	-0.059	0.094	0.419	2.665	15680
37202	B2 IVp	—	—	—	—	21480
37490	B3 III	-0.016	0.060	0.184	2.576	20200
41335	B2 Vne	0.031	0.020	0.002	2.463	20230
43285	B6 Ve	-0.055	0.104	0.481	2.670	14840
44458	B1 Vpe	—	—	—	—	26600
45542	B6 III	-0.049	0.106	0.544	2.657	14080
47054	B8 Ve	-0.022	0.096	0.698	2.677	12500
50658	B8 IIIe	-0.015	0.086	0.596	2.626	13600
50820	B3 IVe+	—	—	—	—	17900
52918	B1 V	-0.072	0.063	0.021	2.591	24720
53416	B8	—	—	—	—	12000
58050	B2 Ve	-0.087	0.081	0.169	2.495	20260
58343	B2 Vne	0.011	0.073	0.264	2.566	18600
58715	B8 Ve	-0.037	0.124	0.791	2.729	11700
60855	B2/B3 V	-0.017	0.059	0.194	2.609	19984
61224	B8/9 IV	0.041	0.061	0.773	2.656	12000
65875	B2.5Ve	0.004	0.040	0.102	2.451	22540
71072	B4 IV	—	—	—	—	16550
91120	B8/9 IV/V	0.005	0.095	0.956	2.742	10600
109387	B6 III pe	-0.023	0.072	0.351	2.566	16850
138749	B6 Vnne	-0.040	0.083	0.479	2.683	14910
142926	B9 pec	-0.029	0.109	0.764	2.677	12000
142983	B8 Ia/Iab	-0.022	0.081	0.664	2.590	12860
143275	B0.2 IVe	-0.016	0.036	-0.020	2.605	26700
162428	A0	—	—	—	—	12200
162732	Bp she	-0.045	0.096	0.786	2.669	11740
164284	B2 Ve	0.057	0.022	0.001	2.495	21650
164447	B8 Vne	-0.013	0.095	0.660	2.721	12900
183362	B3 Ve	-0.009	0.056	0.184	2.528	20260
183656	B6 sh	0.050	0.037	0.809	2.641	11700
183914	B8 Ve	-0.030	0.109	0.725	2.737	12270
187567	B2.5 IVe	0.052	0.007	0.093	2.531	23110
189687	B3 IVe	-0.057	0.081	0.281	2.635	17980
191610	B2.5 Ve	-0.039	0.062	0.162	2.553	20600
192044	B7 Ve	-0.032	0.086	0.603	2.632	13460
193911	B8 IIIne	-0.015	0.073	0.644	2.627	13100
210129	B7 Vne	-0.024	0.101	0.476	2.643	15000
212571	B1 Ve	—	—	—	—	23300
214168	B2 Ve	-0.045	0.055	0.024	2.609	24790
216057	B5 Vne	-0.013	0.088	0.470	2.671	15090
216200	B3 IVne	0.100	0.040	0.331	2.634	17600
217050	B4 IIIep	-0.006	0.062	0.472	2.501	15090
217543	B3 Vpe	-0.034	0.079	0.241	2.650	18860
217675	B6 Ve	0.002	0.042	0.477	2.650	15050
217891	B6 Ve	-0.050	0.109	0.476	2.630	14910

range of 4300–6800 Å with a resolution $R = 21\,000$. The spectra were recorded on a thinned, back-illuminated (SITE) CCD with 1024×1024 pixels of 24 μm size, whose typical readout noise is of about 8 e⁻ and the gain is 2.5 e⁻/ADU. All the spectra have been acquired during several observing runs spanning two years between 2008 and 2009.

The reduction of spectra, which included the subtraction of the bias frame, trimming, correcting for the flat-field and the scattered light, the extraction of the orders, and the wavelength

¹ <http://simbad.u-strasbg.fr/simbad/>

Table 2. Adopted astrophysical quantities for our stars and final best-fit parameters. For each star we report, the number of spectra collected, their classification (abs means absorption lines only), the projected equatorial rotational velocity as measured by us in our spectra, mass and radius as estimated from Drilling & Landolt (1999), peaks separation, critical velocity, equatorial velocity, inclination angle, base density at the stellar equator, and the estimated disk radius. In the last column we also reported the references of other similar catalogs in which spectra of the star have been published: 1) Hanuschik (1988), 2) Hanuschik et al. (1996), 3) Hanuschik (1996), 4) Slettebak et al. (1992), 5) Saad et al. (2006), 6) Silaj et al. (2010).

HD	HR	Name	N	Cl.	$v \sin i$ (km/s)	M_* (M_\odot)	R_* (R_\odot)	Δv_{peak} (km s $^{-1}$)	v_c (km s $^{-1}$)	v_{eq} (km s $^{-1}$)	i ($^\circ$)	ρ_0 (g cm $^{-3}$)	R_d/R_*	rem
6811	335	ϕ And	3	2	80	4.0	3.1	—	500	400	12	$8.50 \cdot 10^{-14}$	6.4	3,5
10516	496	ϕ Per	1	2	240	17.0	10.0	180	570	450	22	$4.20 \cdot 10^{-12}$	4.3	3,4,5
11415	542	ϵ Cas	1	abs	40	6.5	4.2	—	—	—	—	—	—	—
37202	1910	ζ Tau	2	2	120	10.5	6.1	290	—	—	—	—	—	1,2,3,4,5
37490	1934	ω Ori	2	1	180	8.9	5.1	190	580	460	23	$8.00 \cdot 10^{-12}$	3.1	1,2,3,4
41335	2142	V696 Mon	2	2	310	8.9	5.1	—	—	—	—	—	—	1,2,3
43285	2231	—	1	abs	230	6.0	4.0	—	—	—	—	—	—	—
44458	2284	FR CMa	1	2	180	18.0	10.5	150	570	460	23	$3.00 \cdot 10^{-12}$	5.0	3
45542	2343	ν Gem	1	sh	160	5.1	3.5	175	—	—	—	—	—	2,3,4
47054	2418	—	1	1	180	4.0	3.1	140	500	400	27	$3.80 \cdot 10^{-13}$	5.8	3
50658	2568	ψ 09 Aur	1	sh	230	4.5	3.3	150	510	400	80	$3.50 \cdot 10^{-14}$	8.5	3,5
50820	2577	—	1	2	150	7.4	4.6	—	550	440	20	$7.20 \cdot 10^{-14}$	13.8	—
52918	2648	19 Mon	1	abs	240	17.0	10.0	—	—	—	—	—	—	—
53416	—	—	1	1	190	4.0	3.5	120	470	370	30	$7.60 \cdot 10^{-14}$	9.1	—
58050	2817	—	3	1	110	9.0	5.3	—	—	—	—	—	—	3,5
58343	2825	FW CMa	1	2	50	7.5	4.7	—	550	440	6	$1.10 \cdot 10^{-13}$	13.7	2,3,4
58715	2845	β CMi	3	1	210	3.8	3.0	130	490	390	32	$1.25 \cdot 10^{-13}$	7.0	2,3,4,5
60855	2921	V378 Pup	1	2	240	9.0	5.3	150	—	—	—	—	—	2,3
61224	2932	—	2	1	200	4.0	3.1	150	500	400	30	$3.50 \cdot 10^{-13}$	6.2	3
65875	3135	V695 Mon	3	2	180	12.0	7.0	—	—	—	—	—	—	2,3
71072	—	—	2	abs	100	6.5	4.5	—	—	—	—	—	—	—
91120	4123	—	9	1	250	3.0	2.5	180	480	380	41	$1.15 \cdot 10^{-13}$	6.8	2,3
109387	4787	κ Dra	13	1 \leftrightarrow 2	170	7.0	4.5	140	540	430	23	$4.00 \cdot 10^{-12}$	5.1	3,5
138749	5778	θ CrB	11	abs	310	6.0	4.0	—	—	—	—	—	—	5
142926	5938	V839 Her	10	sh	275	4.0	3.1	240	500	400	44	$6.00 \cdot 10^{-12}$	4.3	5
142983	5941	48 Lib	13	sh	390	4.1	3.2	—	—	—	—	—	—	2,3
143275	5953	δ Sco	4	2	165	18.0	10.5	—	—	—	—	—	—	6
162428	—	—	5	1	240	4.0	3.0	180	500	400	36	$9.00 \cdot 10^{-12}$	6.1	4
162732	6664	ζ Her	6	sh	40	3.8	3.0	260	—	—	—	—	—	3,5
164284	6712	66 Oph	6	1	240	10.5	6.1	150	570	460	32	$8.80 \cdot 10^{-14}$	9.3	2,3
164447	6720	V974 Her	4	1	180	4.0	3.5	140	470	370	28	$1.75 \cdot 10^{-13}$	5.8	5
183362	7403	V558 Lyr	4	2	220	9.0	5.3	—	—	—	—	—	—	3
183656	7415	V923 Aql	5	sh	190	3.8	3.0	250	—	—	—	—	—	2,3
183914	7418	β Cyg B	5	1	240	4.0	3.0	160	500	400	37	$9.00 \cdot 10^{-14}$	8.2	3,4
187567	7554	V1339 Aql	4	1 \rightarrow 2	200	13.0	7.7	140	570	450	26	$3.00 \cdot 10^{-13}$	7.3	—
189687	7647	25 Cyg	6	sh	230	7.5	4.7	250	550	440	31	$3.05 \cdot 10^{-13}$	3.6	3,4
191610	7708	28 Cyg	4	1	250	9.0	5.3	270	570	455	33	$2.60 \cdot 10^{-13}$	3.9	3,4
192044	7719	20 Vul	3	1	240	4.5	3.3	150	510	410	38	$1.10 \cdot 10^{-13}$	10.1	—
193911	7789	25 Vul	3	1	170	4.0	3.5	100	470	370	27	$2.30 \cdot 10^{-13}$	6.0	2,3,5
210129	8438	25 Peg	8	1	130	6.0	4.0	70	530	430	19	$1.50 \cdot 10^{-12}$	5.6	1,2,3
212571	8539	π Aqr	3	1	220	13.0	7.7	280	570	450	41	$6.00 \cdot 10^{-13}$	3.9	1,2,3,4
214168	8603	8 Lac B	3	2	150	17.0	10.0	—	—	—	—	—	—	—
216057	8682	—	4	abs	260	6.0	4.0	—	—	—	—	—	—	—
216200	8690	14 Lac	3	sh	195	13.0	7.7	—	—	—	—	—	—	5
217050	8731	—	1	sh	240	6.0	4.0	—	—	—	—	—	—	3,4,5
217543	8758	V378 And	2	sh	305	7.5	4.7	—	—	—	—	—	—	—
217675	8762	ϕ And	2	sh	200	6.0	4.0	—	—	—	—	—	—	4,5
217891	8773	β Psc	6	2	75	6.0	4.0	—	535	430	10	$5.20 \cdot 10^{-13}$	6.1	1,2,4,5

calibration, was done by using the NOAO/IRAF package². The amount of scattered light correction was about 10 ADU. After dividing the extracted spectra by flat-field, the residual shape the spectrum was removed by dividing each spectral order by a Legendre function of a low order. Typical S/N of our spectra is

~ 100 . For some stars this limit has not been reached because its apparent magnitude is close to $V \approx 7$, in which case the S/N was about 50.

Finally, the IRAF package `rvcorrect` was used to include the velocity correction due to the Earth's motion, which moved the spectra into the heliocentric rest frame. The task `splot` and its facilities were used to measure the peaks separation in the H α profile. Errors in the pixels position were converted in errors on the separations, and were evaluated in ≈ 20 km s $^{-1}$.

² IRAF is distributed by the National Optical Astronomy Observatory, which is operated by the Association of Universities for Research in Astronomy, Inc.

Table 3. Program stars for which we have more than two spectra. We reported for both lines mean equivalent widths, their F values, computed according Eq. 3, and the confidence levels of the detected variability.

HD	H α			H β		
	EW(Å)	F	C	EW(Å)	F	C
6811	0.87±0.28	1.84	0.65	6.45±0.09	1.99	0.67
37202	-15.26±1.17	1.41	0.49	2.34±0.01	1.41	0.49
37490	-5.96±1.09	1.41	0.49	1.83±0.18	1.41	0.49
41335	-31.92±0.78	1.41	0.49	-1.44±0.52	1.41	0.49
58050	-4.40±0.31	1.94	0.66	5.49±0.04	1.73	0.63
58715	-1.19±0.36	1.94	0.66	7.96±0.06	1.98	0.66
61224	-5.59±0.48	1.41	0.49	5.14±0.40	1.41	0.49
65875	-43.00±0.89	1.90	0.66	0.04±0.60	1.77	0.64
71072	3.14±0.08	1.41	0.49	5.22±0.23	1.41	0.49
91120	-0.40±0.50	3.49	0.92	8.07±0.15	3.21	0.91
109387	-19.17±0.44	3.58	0.94	3.04±0.06	2.85	0.90
142926	-1.63±0.45	3.68	0.93	7.05±0.13	3.06	0.90
142983	-24.66±0.86	3.31	0.93	3.09±0.14	3.85	0.95
143275	-10.13±2.29	2.34	0.76	-0.81±0.20	2.30	0.75
162428	-15.57±0.14	2.44	0.80	4.78±0.38	2.40	0.80
162732	-6.61±0.88	2.52	0.83	5.92±0.50	2.89	0.85
164284	1.37±1.57	2.71	0.84	5.18±0.08	2.64	0.84
164447	-0.95±1.13	2.64	0.81	6.68±0.15	2.68	0.82
183362	-26.39±0.15	1.88	0.65	1.25±0.15	1.79	0.64
183656	-7.68±0.72	2.50	0.80	5.15±0.18	2.28	0.80
183914	-0.94±0.22	2.78	0.82	8.10±0.07	2.53	0.80
187567	-21.82±0.66	2.14	0.74	0.56±0.19	2.21	0.74
189687	0.93±0.25	2.93	0.86	4.76±0.05	3.11	0.87
191610	0.12±0.24	2.03	0.72	4.69±0.15	2.04	0.72
192044	-9.96±0.13	1.97	0.66	5.25±0.05	1.96	0.66
193911	-5.45±0.13	1.95	0.66	5.10±0.05	1.89	0.65
210129	-14.17±0.21	3.26	0.90	5.11±0.15	3.13	0.89
212571	-5.40±0.04	1.99	0.67	1.98±0.14	1.98	0.66
214168	-14.79±0.35	2.00	0.67	1.87±0.52	1.82	0.65
216057	4.62±0.15	2.36	0.76	7.19±0.10	2.21	0.74
216200	1.15±0.43	1.98	0.66	5.08±0.21	1.97	0.66
217543	2.35±0.76	1.41	0.49	5.31±0.11	1.41	0.49
217675	3.05±0.28	1.41	0.49	5.64±0.18	1.41	0.49
217891	-12.94±0.64	2.70	0.84	4.70±0.19	2.70	0.84

For each spectrum we measured the equivalent widths (including underlying absorption) of both H α and H β , where a negative value means the corresponding line shows net emission. All the measured equivalent widths are reported in Table B.1.

3. Classification and fit of the H α line profiles

Almost all the stars in our sample were found with emission in the H α . Then, considering the shape of their profile and according to the classification scheme proposed by Hanuschik (1988), we classified our stars as belonging to

- class 1 when they exhibit a rather symmetrical double peak structure with $V/R \approx 1$,
- class 2 when they have an asymmetric single peak or a dominant peak with a much weaker secondary peaked,
- shell stars when the central reverse is deeper than the continuum level,
- *abs* when there is not emission above the continuum level.

Our classification is reported in the fourth column of Table 2.

Only for the stars belonging to class 1, plus stars from other classes but with V/R ratio close to unity, we attempt an estimation of the disk dimension. The approach we used was to minimize the difference between observed and synthetic profiles,

computed in two separate steps. First of all, we calculated the photospheric H α , then the contribution due to the net emission of the disk and then we added these two synthetic profiles obtained separately. These two steps are described in the following:

– Computation of the photospheric profile

We first computed the photospheric H α profiles for all our program stars. They were generated in three steps: *i*) first, we computed an LTE model atmosphere using the ATLAS9 code (Kurucz 1993), *ii*) the stellar spectrum was then synthesized using SYNTHE (Kurucz & Avrett 1981), and *iii*) the spectrum was convolved with the instrumental and rotational profiles.

First of all we had to obtain an estimation of the effective temperature for each target. Considering that the continuum energy distribution of Be stars is typical of normal early-type stars both in the visual and UV, but not in the IR, where an excess could be present because of the hot circumstellar dust (Zickgraf 2000), effective temperatures were computed from Strömgren photometry (Hauck & Mermilliod 1998) using the algorithm coded by Moon (1985), with the exception of eight stars for which photometry is not available. This method is allowed because it does not involve any IR filter. For seven of them we adopted the temperatures from the literature: HD 10516, HD 37202, and HD 44458 from Soubiran et al. (2010), HD 58020 and HD 71072 from Hohle et al. (2010), HD 162428 from Moujtahid et al. (1999), and HD 212571 from Wu et al. (2011), while for HD 53416 we derived an estimation of temperature from spectral type and the calibration by Kenyon & Hartman (1995). Since our targets have luminosity class IV/V (as reported in the SIMBAD database), we fixed the surface gravity to $\log g = 4.0$, except for HD 11415, HD 37490, HD 45542, HD 50658, HD 109387, HD 193911, and HD 217050 (luminosity class III) for which $\log g = 3.0$ has been preferred. Radii and masses were adopted following the calibration in Drilling & Landolt (1999). Assuming these atmospheric parameters, we computed the $v \sin i$ of each star by spectral synthesis of the observed MgI $\lambda 4481$ Å. This line was chosen because in the spectral range of our targets, it reaches its maximum depth and therefore it is better suited to determining the rotational velocity. Errors on the projected rotational velocities are $\approx 15 \text{ km s}^{-1}$.

– Computation of net disk emission

We have adopted the Be disk model approach of Hummel & Vrancken (2000) that is based on models developed by Horne & Marsh (1986) and Horne (1995) for accretion disks in cataclysmic variables. The disk is assumed to be axisymmetric and centered over the equator of the underlying star, and the gas density varies as

$$\rho(R, Z) = \rho_0 R^{-n} \exp \left[-\frac{1}{2} \left(\frac{Z}{H(R)} \right)^2 \right]$$

where R and Z are the radial and vertical cylindrical coordinates (in units of stellar radii), ρ_0 is the base density at the stellar equator, n a radial density exponent, and $H(R)$ the disk vertical scale height. The neutral hydrogen population within the disk is found by equating the photo-ionization and recombination rates (Gies et al. 2007). The disk gas is assumed to be isothermal and related to the stellar effective temperature T_{eff} by $T_d = 0.6 T_{\text{eff}}$ (Carciofi & Bjorkman 2006).

This approach takes the contribution of the central star's finite size on the H α line formation process into account, i.e. the

obscuration of the disk by the central star at any given inclination. The numerical model represents the disk by a large grid of azimuthal and radial surface elements, and the equation of transfer is solved along a ray through the center of each element according to

$$I_\lambda = S_\lambda^L (1 - e^{-\tau_\lambda}) + I_\lambda^S e^{-\tau_\lambda}$$

where I_λ is the derived specific intensity, S_λ^L the source function for the disk gas (taken as the Planck function for the disk temperature T_d), I_λ^S the specific intensity for the H α of the star, and τ_λ the integrated optical depth along the ray. The first term applies to all the disk area elements that are unocculted by the star, while the second term applies to all elements that correspond to the projected photospheric disk of the star. The absorption line adopted in I_λ^S is Doppler-shifted according to solid-body rotation for the photospheric position in a star that is rotating at 80% of the critical value.

Electron scattering is not taken into account in the line profile computation. So we do not expect to reproduce the wings of strong lines well, since for these lines the broadening of the wings due to the electron scattering can not be neglected. Disk kinematic is taken into account using a rotational velocity law written as

$$V(R) = V_{\text{rot}}^* R^{-j}$$

(Hutchings 1970), where R represents the radial coordinate that has its origin at the center of the star, and V_{rot}^* denotes the actual rotational velocity at the stellar surface. The exponent ranges from $j = 1/2$ for pure Keplerian rotation and $j = 1$ corresponding to conservation of angular momentum. Likewise the value of j is still matter of debate, recent studies seem to converge toward the Keplerian value (Hummel & Vrancken 2000, Meilland et al. 2007). Thus, in this study we assumed the disk to be in pure Keplerian rotation.

Once we obtained and combined these two contributions, we started the minimization algorithm using as goodness-of-fit test the parameter

$$\chi^2 = \frac{1}{N} \sum \left(\frac{I_{\text{obs}} - I_{\text{th}}}{\delta I_{\text{obs}}} \right)^2$$

where N is the total number of points, I_{obs} and I_{th} are the intensities of the observed and computed profiles, respectively, and δI_{obs} is the photon noise.

As initial guesses for the inclination angle i and for the disk radius, we used the equations

$$v_{\text{eq}} \sin i = 0.8 \sqrt{\frac{GM_*}{R_*}} \sin i \quad (1)$$

where $v_{\text{eq}} \sin i$ is the value measured in our spectra, and

$$\frac{\Delta v_{\text{peak}}}{2 v \sin i} = r_d^{-j} \quad (2)$$

(equation [6] in Hanuschik et al. (1988)) where Δv_{peak} is the separation between violet and red peaks, as measured in each profile and reported in Table 2.

Then, fine tuning was carried out using the *amoeba* minimization³ algorithm between observed and computed profiles.

³ The *amoeba* routine implements the simplex method of Nelder & Mead (1965).

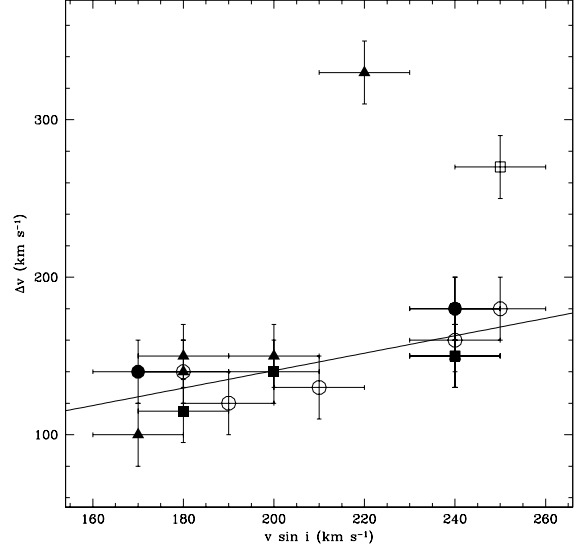


Fig. 2. Correlation between measured $v \sin i$ and peaks separation. The points have been grouped on the basis of the mean equivalent width: $EW \leq -20 \text{ \AA}$ (filled squares), $-20 \text{ \AA} < EW \leq -15 \text{ \AA}$ (filled circles), $-10 \text{ \AA} < EW \leq -5 \text{ \AA}$ (filled triangles), $-5 \text{ \AA} < EW \leq 0 \text{ \AA}$ (open circles), and $EW \geq 0 \text{ \AA}$ (open squares).

In our procedure two assumptions have been made: radial density exponent has been fixed to $n = 3$ and, as stated before, the Keplerian rotation of the disk has been considered ($j = 1/2$). The first hypothesis, regarding the value of the density exponent can be justified by considering the work of Grundstrom & Gies (2006). These authors computed several theoretical curves that described the dimension of the disk radius as a function of the H α equivalent width, for different values of the inclination angle i and different values of n . They concluded that the overall shape of those curves for different n and equal i are almost the same, since it is a small difference of $\approx 3\%$ in correspondence of equivalent widths between -2 and -15 \AA when n change from 3 to 3.5. They then suggest that the particular choice of n is not as important as the choice of the right i . Moreover, Porter & Rivinius (2003) from IR flux excess in Be stars suggested that n falls in the interval $n = 2 \div 4$. Thus, on the basis of these results, we fixed the value of the density exponent to the middle value of $n = 3$. Total H α profiles, star+disk, are presented in Figs. A.1, A.2, and A.3.

To derive an estimation of the disk radius, we used the method developed by Grundstrom & Gies (2006) to form a synthetic image of the system star+disk in the plane of sky by summing the intensity over a 2.8 nm band centered on H α . We collapsed this image along the projected major axis to get the summed spatial intensity, and we adopted the value for which the summed intensity drops to half its maximum value as effective disk radius.

We estimated the errors on the disk dimensions and on the inclination angles to be $\pm 2 R_*$ and $\pm 3^\circ$, respectively. These determinations have been estimated by varying in Eqs. 1 and in 2 the observed quantities $v \sin i$ and peak separation by their experimental errors and considering as uncertainties the semi-amplitude of this variation.

All the adopted and derived parameters are reported in Table 2.

4. H α and H β Variability

Usually Be stars display variability in their equivalent width (EW) and/or in their spectral profile.

To find whether a star presents equivalent width variation, we applied to both H α and H β equivalent widths the statistical method called F-test. When more than one observation was present for a given target, we calculated the amplitude of the variation, ΔEW , and the standard deviation of the sample using

$$\sigma = \sqrt{\frac{1}{N-1} \sum (EW_i - \overline{EW})^2}$$

where N is the number of points, and the (N-1) corresponds to the degree of freedom used for the F-test. Having obtained ΔEW and σ , we calculated a simple observable to assess the variability for a given target using a ratio of the form:

$$F = \frac{\Delta EW}{\sigma}. \quad (3)$$

This simple ratio represents the number of times that the amplitude of the variation is greater than the standard deviation.

To determine whether or not this number is meaningful and whether the star shows variability, we evaluated the corresponding confidence level; see last column of Table 3. We considered all the stars for which $C \geq 80\%$ as definitively variable (13 stars, that is 41% of the sample), while we cannot say anything for the target with $C \leq 50\%$ (22% of the sample) due to the small number of points. The 37% of the stars, are probably variable but within a confidence level ranging from 50% to 80%. In any case, all the targets show the same behavior in both spectral lines.

In this atlas we show the full set of our profiles (H α and H β) for the 48 observed stars. In Figs. B.1 to B.5, we show the Balmer profiles observed for program stars with multiple measurements. In each panel we reported for each profile also the last four digits of the heliocentric julian date of the observation. In some cases to improve the visualization, profiles have been blown up according to

$$F'_\lambda = [(F_\lambda - 1) * k] + 1 \quad (4)$$

where F_λ denotes the observed flux, F'_λ the displayed flux, and k is the magnification factor.

In Fig. B.7 we show all the stars for which we collected one spectrum only. Most of the stars have been measured several times during the 2008/2009 period, but only few stars showed significant variations in their spectral profiles. These objects are discussed separately in the following:

HD 37202 - This star has been observed in two nights separated by 205 days. It is clearly visible an increase in flux in the violet peak in both spectral lines, even if it is more evident in H β .

HD 41335 - As for the previous object, only two observations have been acquired for this star in a range of 207 days. The star exhibits V/R variations in both lines.

HD 58050 - The triple-peaked structure visible in the H α observed in the first night is missing in the other two spectra. No features are seen in the H β .

HD 109387 - This star was observed for 13 nights in a period spanning 110 days. The top part of the H α emission profiles shows irregular variability, with back and forth changing from class 2 toward class 1, but no evident sign of day-by-day variability has been observed. No variations have been detected in H β double-peaked profile.

HD 142926 - During 110 days this shell star was observed 10 times showing a slight V/R variability in the H α .

HD 143275 - In the four spectra acquired by us, δ Sco shows important changes in the emission of H α . The V/R changes over the observational period and it shows a flat core in the first spectrum.

HD 164284 - Observed for six times in 536 days, this star exhibits equivalent width variability. The double-peaked emission of the H α profile decrease with time, although the V/R remains constant and ≈ 1 . Also the H β shows a change in the shape, since it is the last profile without any peak.

HD 183362 - This star shows an increased emission level on the red side of its profile.

HD 183656 - V/R variability has been observed, both in H α and in H β profiles, in the six spectra acquired in a range of 358 days.

HD 187567 - This star show variability in the H α profile, and evolves from class 1 toward class 2.

HD 189687 - In the H α , this star does not show any sign of variability for the first month of observations. In the last spectrum taken after 32 days from the second to last, it starts to show an increase of the flux in the red peak. No H β variability has been detected.

HD 191610 - This star shows a gradual increment of the flux in the red peak.

5. Discussion and conclusions

In this paper we presented a homogeneous sample of H α and H β line profiles observed in 32 Be stars, which show emission at least in the H α line. According to Hanuschik (1988), we classified our targets on the basis of the following scheme:

- 16 stars, 33% of the sample, in class 1;
- 13 stars, 27% of the sample, in class 2;
- 11 stars, 23% of the total, has been classified as shell stars;
- 6 stars, 12% of the total, do not show net emission.

In this list we do not include the two stars that show any phase transition between classes 1 and 2.

This frequency distribution shows that the majority of our sample of 48 Be stars, randomly distributed in spectral type, belongs to class 1 profiles. Regarding the 13 stars classified as class 2, seven of them are single peak, while six show structured profiles.

Two stars showed variability from one class to another. HD 187567 has undergone an evolution from class 1 to class 2, while the behavior of HD 109387 is more complicated. In 110 days, this star has been observed 13 times, and it showed a transition from class 2 to class 1 and back again to class 2.

In Fig. 2 we compared the behavior of the H α peaks separation to $v \sin i$ for the stars of the class 1 (included the class 2 HD 60855). A linear correlation seems to exist, as expected from the work of Hanuschik et al. (1988), although two stars discarded from this trend, namely HD 191610 and HD 212571. To verify this correlation we computed the Pearson r coefficient, obtaining $r = 0.72$ and the linear fit given by the equation:

$$y = (0.56 \pm 0.13) \cdot x + (29.94 \pm 26.80). \quad (5)$$

Thus, we confirm that $v \sin i$ and H α peaks separation are in linear correlation, confirming the disk-like geometry of Be star envelopes and, probably this assumption is not valid for HD 191610 and HD 212571.

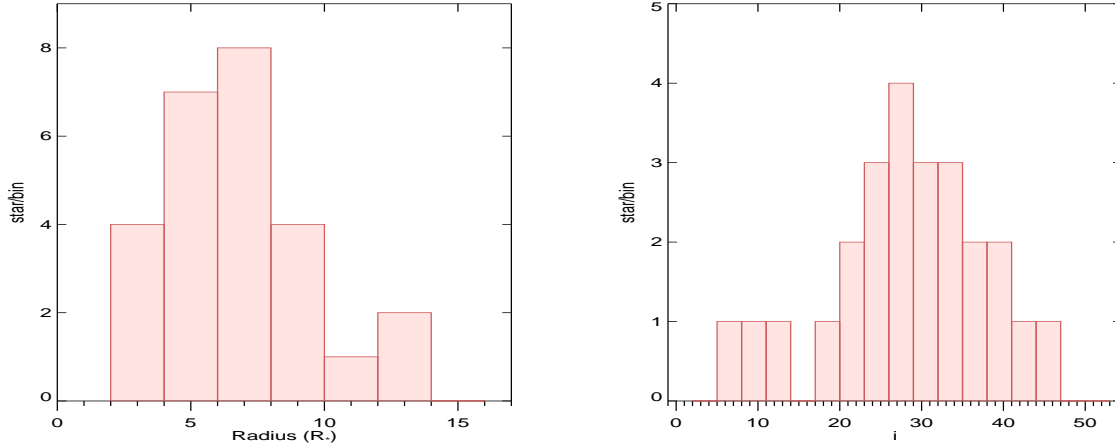


Fig. 3. Histograms of distribution of stars as a function of the dimension of their disks (left panel) and of the inclination angles (right panel). To build these histograms we chose a bin size of $2 R_*$ and 3° , respectively.

For all the stars belonging to the class 1, we attempted to model the emission with the purpose of deriving some parameters such inclination angle, base density at the stellar equator and disk radius. In Fig. 3 we show the distribution of stars as a function of the disk radius (right panel) and of the inclination angle (left panel). The histograms were built considering a binning equal to the estimated errors, that is, $2R_*$ and 3° in the disk dimension and inclination angle, respectively. They show as there is a major concentration of stars for disk around $6 \div 8 R_*$ (about 17% of our sample) and for angles around $23^\circ \div 35^\circ$ (about 28% of the sample).

Moreover, with the aim of inferring line profile variability, for most of the stars of our sample we obtained more than one spectrum in a period spanning two years between 2008 and 2009. All but seven stars, those discussed in Sect. 4, do not show any evident sign of variability in both Balmer lines.

Acknowledgements. This research made use of the SIMBAD database, operated at the CDS, Strasbourg, France.

References

- Carciofi, A. C., & Bjorkman, J. E. 2006, *ApJ*, 639, 1081
 Drilling, J., & Landolt, A. U. 1999, in: *Allen's Astrophysical Quantities*, Fourth Edition, Edited by Arthur N. Cox, Los Alamos, NM
 Gies, D. R., Bagnuolo, W. G. Jr., Baines, E. K., et al. 2007, *ApJ*, 654, 527
 Grundstrom, E. D., & Gies, D. R. 2006, *A&A*, 651, 53
 Hanuschik, R. W. 1996, *A&A*, 308, 170
 Hanuschik, R. W., Hummel, W., Sutorius, E., Dietle, O., & Thimm, G., 1996, *A&ASS*, 116, 309
 Hanuschik, R. W., Kozok J. R., & Kaiser, D. 1988, *A&A*, 189, 1988
 Hauck, B., & Mermilliod, M. 1998, *A&AS*, 129, 431
 Hohle, M. M., Neuhauser, R., & Schutz, B.F. 2010/ *AN*, 331, 349
 Horne, K. 1995, *A&A*, 297, 273
 Horne, K., & Marsh, T. R. 1986, *MNRAS*, 218, 761
 Hummel, W., & Vrancken, M. 2000, *A&A*, 302, 751
 Hutchings, J. B. 1970, *MNRAS*, 150, 55
 Jaschek, M., & Egret, D., 1982, A catalogue of Be stars. In: *Be stars*, IAU Symp. 98, 261 Ed. M. Jaschek and H.-G. Groth, Munich
 Kurucz, R.L. 1993, A new opacity-sampling model atmosphere program for arbitrary abundances. In: *Peculiar versus normal phenomena in A-type and related stars*, IAU Colloquium 138, M.M. Dworetsky, F. Castelli, R. Faraggiana (eds.), ASP Conference Series Vol. 44, p.87
 Kenyon, S. J., & Hartmann, L., 1995, *ApJS*, 101, 117
 Kurucz, R. L., & Avrett, E. H. 1981, *SAO Special Rep.*, 391
 Meilland, A., Stee, Ph., Vannier, M. et al. 2007, *A&A*, 464, 59
 Moon, T. T. 1985, *Comm. from the Univ. of London Obs.*, 78
 Moujtahid, A., Zorec, J., & Hubert, A. M. 1999, *A&A*, 349, 151
 Nelder, J. A., & Mead, R., 1965, *Computer Journal*, Vol 7, pp 308-313.
 Okazaki, A. T. 1997, *A&A*, 318, 548
 Porter, J. M., & Rivinius, Th., 2003, *PASP*, 115, 1153
 Porter, J. M. 1996, *MNRAS*, 280, L31
 Saad, S.M., Kubát J., Korcáková, D., et al., 2006, *A&A*, 450, 427
 Silaj, J., Jones, C. E., Tycner, C., Sigut, T. A. A., & Smith, A.D., 2010, *ApJS*, 187, 228
 Slettebak, A., Collins, G. W., Truax, R., 1992, *ApJS*, 81, 335
 Soubiran, C., Le Campion, J.-F., Cayrel De Strobel, G., & Caillo, A. 2010, *A&A*, 515, 111
 Struve, O. 1931, *ApJ*, 73, 94
 Wu, Y., Singh, H. P., Prugnel, P., Gupta, R., & Koleva, M. 2011, *A&A*, 525, 71
 Zickgraf, F.-J., 2000, The connection with B[e] stars. In: *The Be phenomenon in Early-Type stars*, IAU Colloquium 175, M. A. Smith, H. F. Henrichs, J. Fabregat (eds), ASP Conference Series Vol. 214, p. 26

Appendix A: Fit emission

Appendix B: Variability

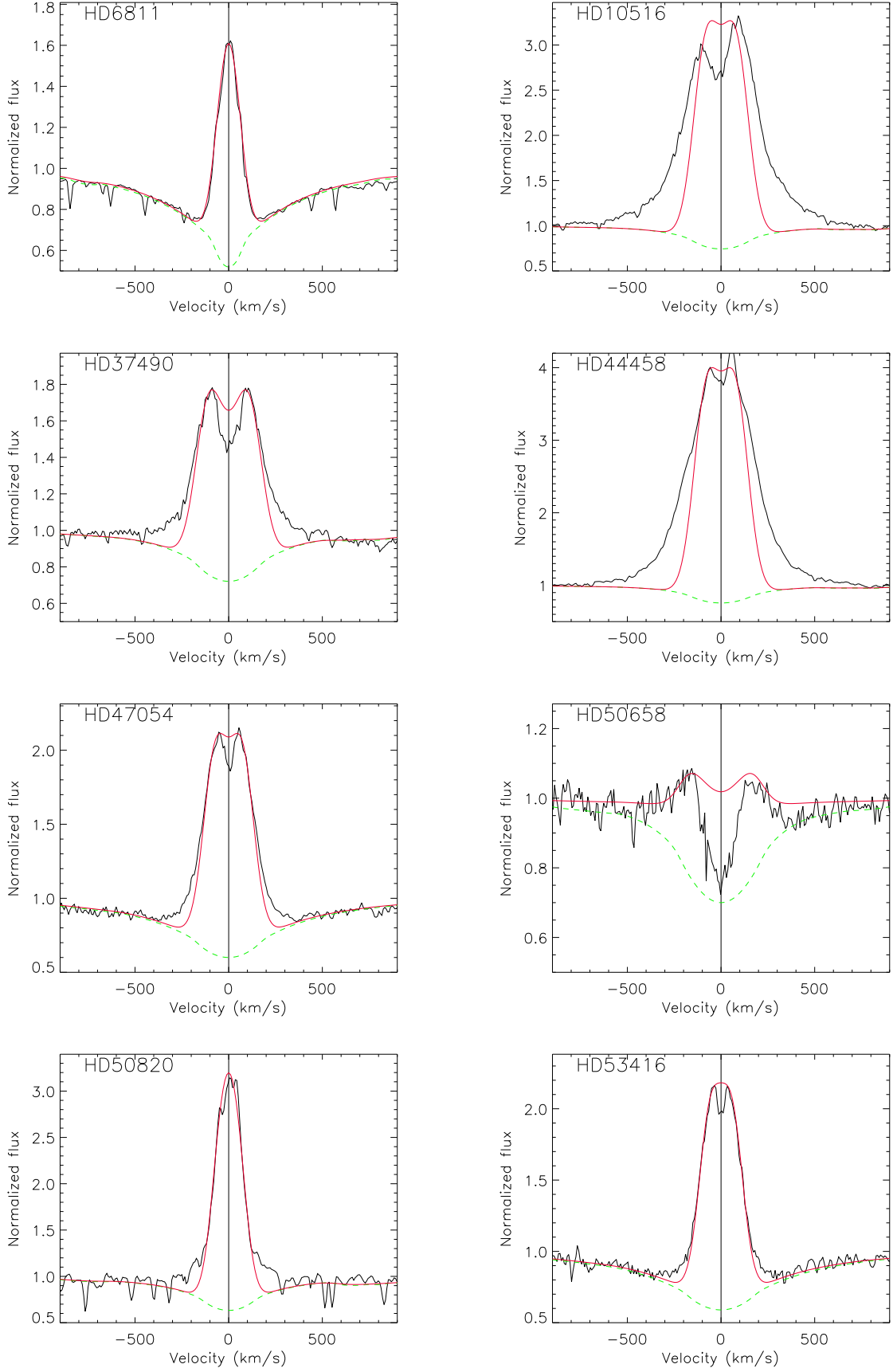


Fig. A.1. Observed $H\alpha$ of Be stars with both stellar absorption (dashed green lines) and total emission profiles (solid red lines) overimposed. Best fit parameters for stellar and disk synthetic profiles are reported in Table 2. The circumstellar emission have been calculated by fixing the radial density exponent ($n = 3$) and considering Keplerian rotation of the disk (i.e. $j = 1/2$)

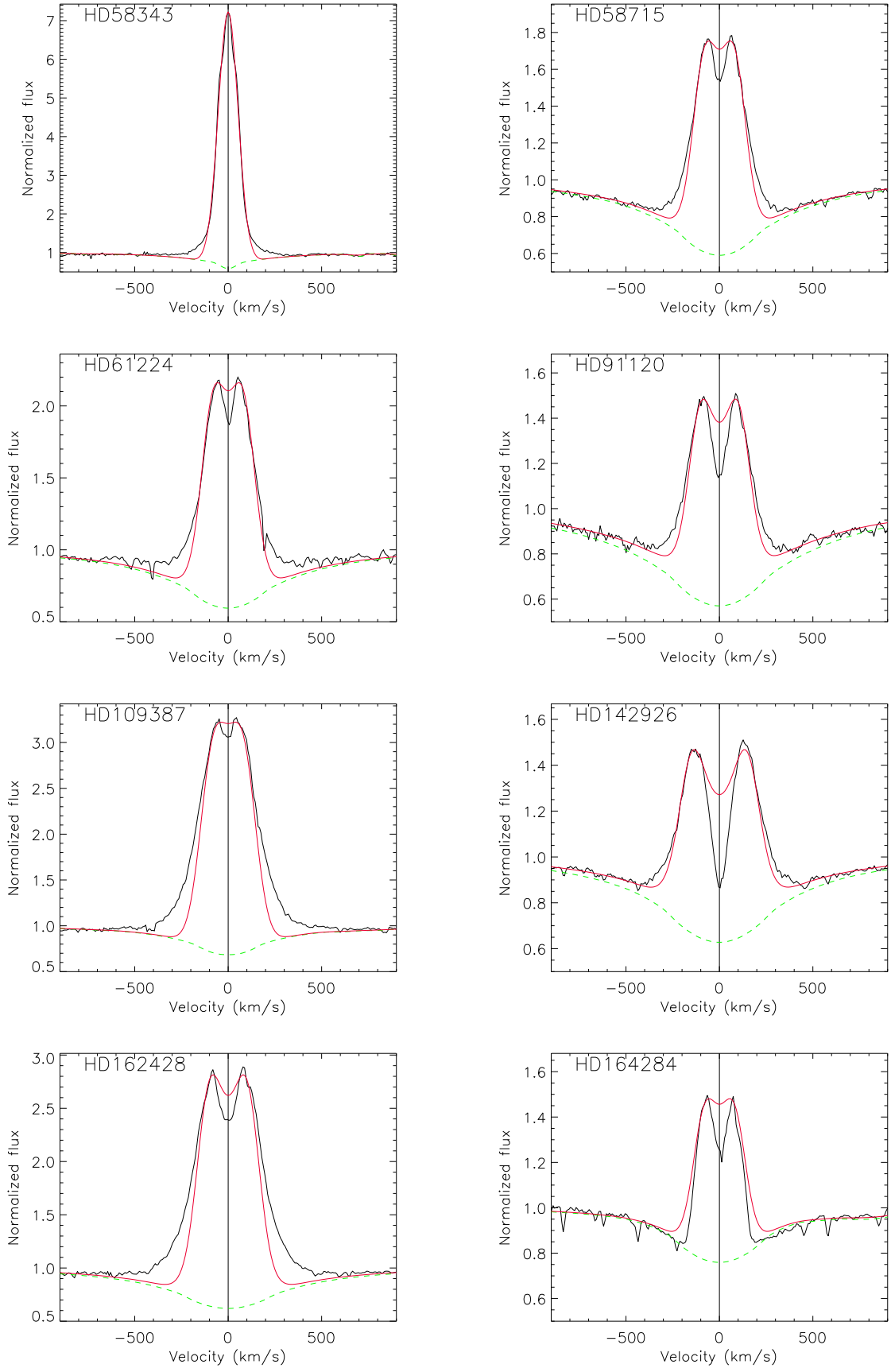


Fig. A.2. As in Fig. A.1

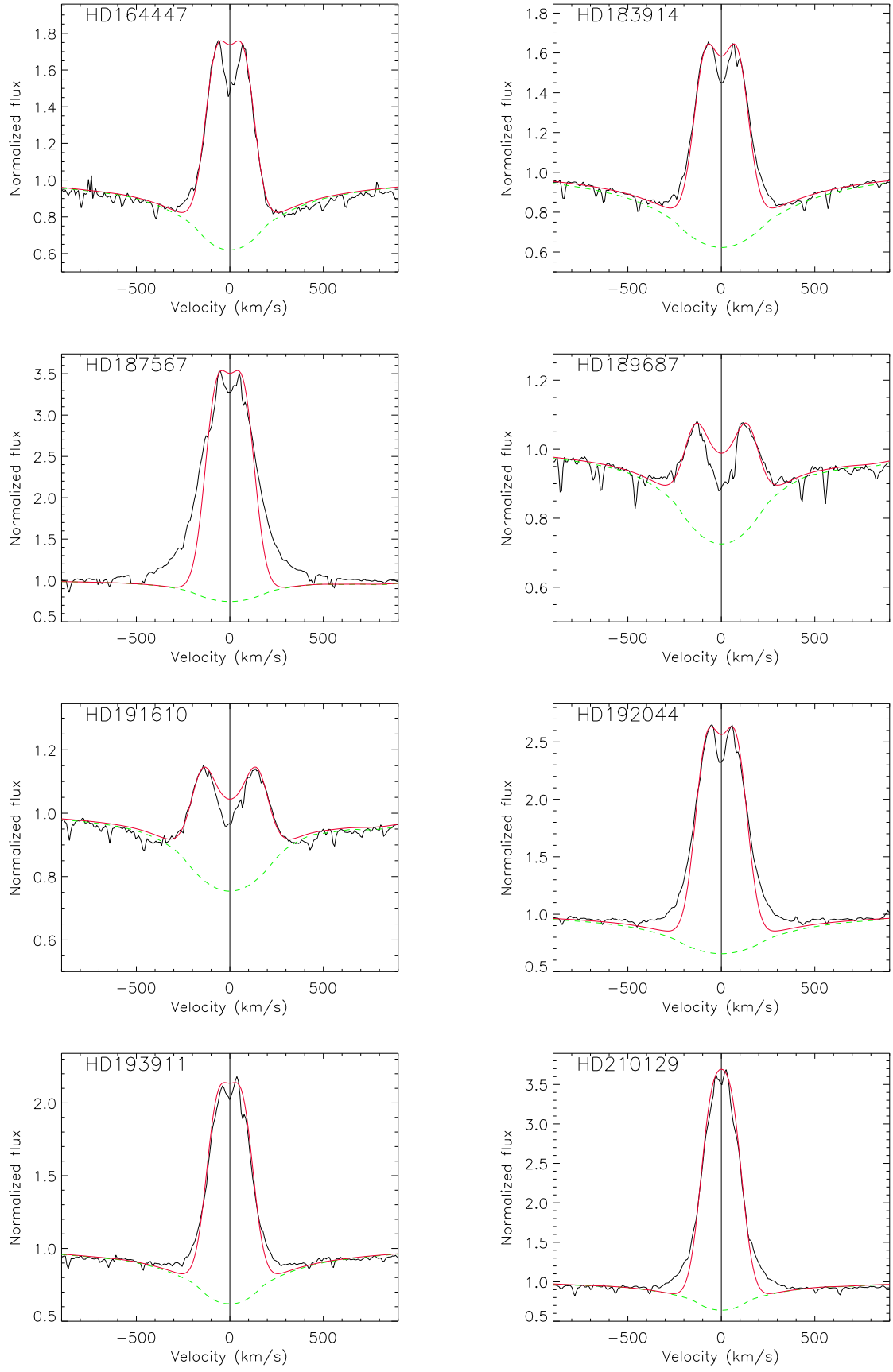


Fig. A.3. As in Fig. A.1

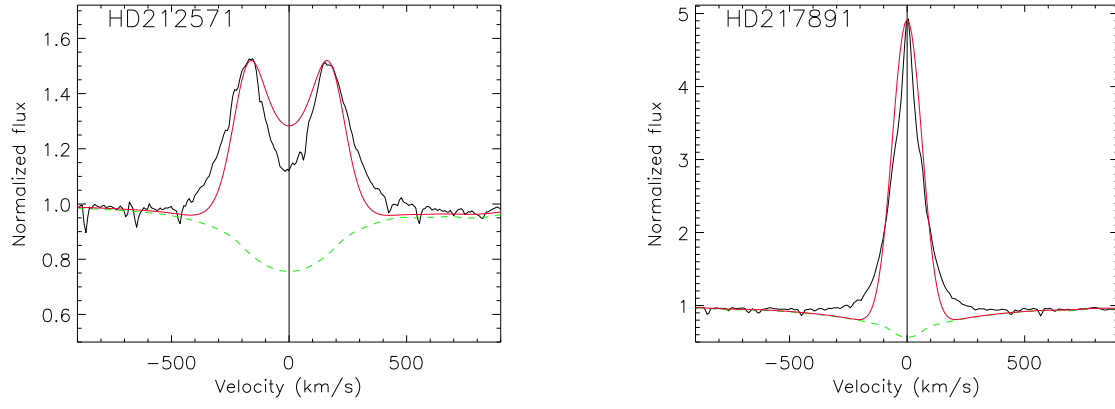


Fig. A.4. As in Fig. A.1

Table B.1. H α and H β equivalent width as measured in our spectra. Negative values mean that the lines show net emission.

HD	JD (2450000+)	EW(Å) H α	EW(Å) H β	HD	JD (2450000+)	EW(Å) H α	EW(Å) H β	HD	JD (2450000+)	EW(Å) H α	EW(Å) H β
6811	4714.6282	1.06	6.53	142926	4543.6113	-2.82	7.14	187567	4654.5327	-21.09	0.81
	4747.5640	0.99	6.46		4554.6243	-1.61	7.04		4655.5890	-21.46	0.59
	4749.6417	0.55	6.36		4555.6541	-1.68	6.84		4678.5234	-22.24	0.40
10516	4749.6602	-25.21	0.37		4556.6487	-1.40	6.80		4714.4153	-22.50	0.44
11415	4749.6753	4.25	5.83		4575.5709	-1.61	7.11	189687	4654.5758	0.76	4.70
37202	4544.2610	-16.09	2.33		4576.5771	-1.68	7.14		4655.5411	0.93	4.75
	4749.7298	-14.44	2.35		4586.5501	-1.49	7.12		4677.5324	0.62	4.77
37490	4544.2799	-5.19	1.95		4588.5402	-1.38	7.05		4681.5430	1.01	4.76
	4749.7175	-6.73	1.70		4616.4682	-1.46	7.03		4682.5777	0.89	4.76
41335	4542.3012	-31.37	-1.81		4653.3880	-1.18	7.20		4714.4602	1.35	4.84
	4749.7436	-32.48	-1.07	142983	4543.5309	-26.32	3.24	191610	4712.3812	0.48	4.81
43285	4543.3009	5.06	7.57		4555.5462	-23.71	3.15		4713.3568	-0.00	4.63
44458	4544.3009	-31.82	-0.80		4556.5508	-24.48	3.08		4747.3386	-0.01	4.81
45542	4542.3231	-0.91	5.93		4575.5004	-24.74	3.03		4749.4744	-0.00	4.51
45725	4542.3417	9.38	11.36		4576.4808	-24.61	3.15	192044	4712.4081	-9.93	5.21
47054	4543.3275	-6.86	6.17		4585.4945	-25.81	3.07		4713.3805	-10.10	5.24
50658	4542.3850	1.34	5.67		4586.4283	-25.08	3.16		4747.3594	-9.84	5.30
50820	4544.3397	-8.32	-2.73		4587.4507	-24.20	2.75	193911	4712.4526	-5.42	5.04
52918	4542.4174	2.77	3.78		4588.4201	-23.85	3.24		4713.4085	-5.34	5.12
53416	4556.2808	-4.66	6.42		4599.4307	-24.62	3.03		4747.3837	-5.60	5.14
58050	4544.3849	4.31	5.44		4616.3757	-25.63	3.05	210129	4654.5979	-13.86	4.85
	4554.2984	4.74	5.51		4653.4399	-23.49	3.29		4677.5640	-14.28	5.02
	4556.3476	4.14	5.51		4654.4038	-24.03	2.97		4678.5672	-14.30	5.24
58343	4543.3636	-19.29	2.75	143275	4677.3348	-11.01	-0.78		4681.5694	-14.18	5.04
58715	4542.4392	-0.79	7.91		4681.3050	-6.94	-0.64		4682.6018	-14.14	5.11
	4554.3634	-1.29	7.95		4682.3327	-10.28	-0.73		4714.4878	-14.01	5.23
	4556.3986	-1.49	8.02		4714.2604	-12.30	-1.09		4747.4096	-14.54	5.33
60855	4543.3894	-38.59	-0.95	162428	4586.5791	-15.50	5.03		4749.5015	-14.04	5.04
61224	4555.2948	-5.93	5.42		4588.5667	-15.72	4.12	212571	4712.4805	-5.37	2.11
	4556.4231	-5.25	4.85		4677.3624	-15.69	4.99		4714.5117	-5.44	2.00
65875	4543.4116	-42.00	-0.28		4681.3258	-15.58	4.80		4749.5255	-5.40	1.83
	4544.4331	-43.32	0.74		5011.4665	-15.38	4.96	214168	4713.4584	-15.13	2.12
	4554.4361	-43.69	-0.33	162732	4586.6250	-7.24	6.13		4747.4338	-14.44	2.22
71072	4555.3404	3.20	5.05		4616.5402	-6.95	5.91		4749.5512	-14.80	1.27
	4576.3047	3.09	5.38		4654.4306	-6.00	6.40	216057	4713.4828	4.48	7.25
91120	4543.4858	-1.39	8.32		4677.4028	-7.04	4.94		4714.5419	4.60	7.15
	4554.3985	-0.31	8.19		4682.3762	-7.31	6.07		4747.4580	4.84	7.29
	4555.4708	-0.40	8.15		5011.5115	-5.09	6.04		4749.5750	4.58	7.07
	4556.4743	-0.52	8.02	164284	4575.5993	-0.01	5.19	216200	4713.5068	1.07	5.04
	4576.3563	-0.66	7.90		4576.6058	-0.00	5.04		4714.5693	1.61	5.31
	4585.3822	-0.66	8.02		4616.5681	0.91	5.23		4749.6007	0.76	4.90
	4586.3393	-0.01	7.84		4677.4774	1.43	5.12	217050	4747.5172	-27.42	1.82
	4587.3192	-0.01	8.05		4682.4266	1.64	5.26	217543	4713.5577	1.81	5.38
	4588.3168	0.37	8.16		5011.5620	4.25	5.23		4747.5433	2.89	5.23
109387	4543.5060	-20.01	3.05	164447	4575.6219	-2.03	6.62	217675	4713.6001	3.24	5.51
	4554.4814	-19.83	3.01		4677.4415	-1.24	6.64		4747.4769	2.85	5.77
	4555.5156	-19.34	3.07		4681.3697	-1.44	6.68	217891	4678.6041	-12.16	4.93
	4556.5191	-19.09	2.97		4749.3442	-1.02	6.93		4681.6008	-12.46	4.86
	4575.4348	-19.43	3.02		5011.5811	0.96	6.52		4713.6187	-12.85	4.76
	4576.4464	-19.42	2.98	183362	4653.5050	-26.22	1.35		4714.6005	-12.80	4.66
	4585.4577	-19.09	3.02		4682.5161	-26.45	1.08		4747.4941	-13.47	4.57
	4586.3921	-19.00	2.98		4714.3334	-26.50	1.33		4749.6231	-13.90	4.42
	4587.3898	-18.78	2.99	183656	4653.5999	-8.27	5.24				
	4588.3867	-18.77	3.07		4681.4527	-7.59	5.25				
	4599.3878	-18.45	3.14		4714.3630	-8.01	5.35				
	4616.3342	-19.11	3.13		4749.3742	-8.07	4.98				
	4653.3303	-18.84	3.12		5011.6055	-6.48	4.94				
				183914	4653.5454	-1.01	8.03				
					4681.4958	-0.91	8.09				
					4682.5518	-0.96	8.20				
					4714.3886	-0.61	8.14				
					4749.4339	-1.23	8.06				

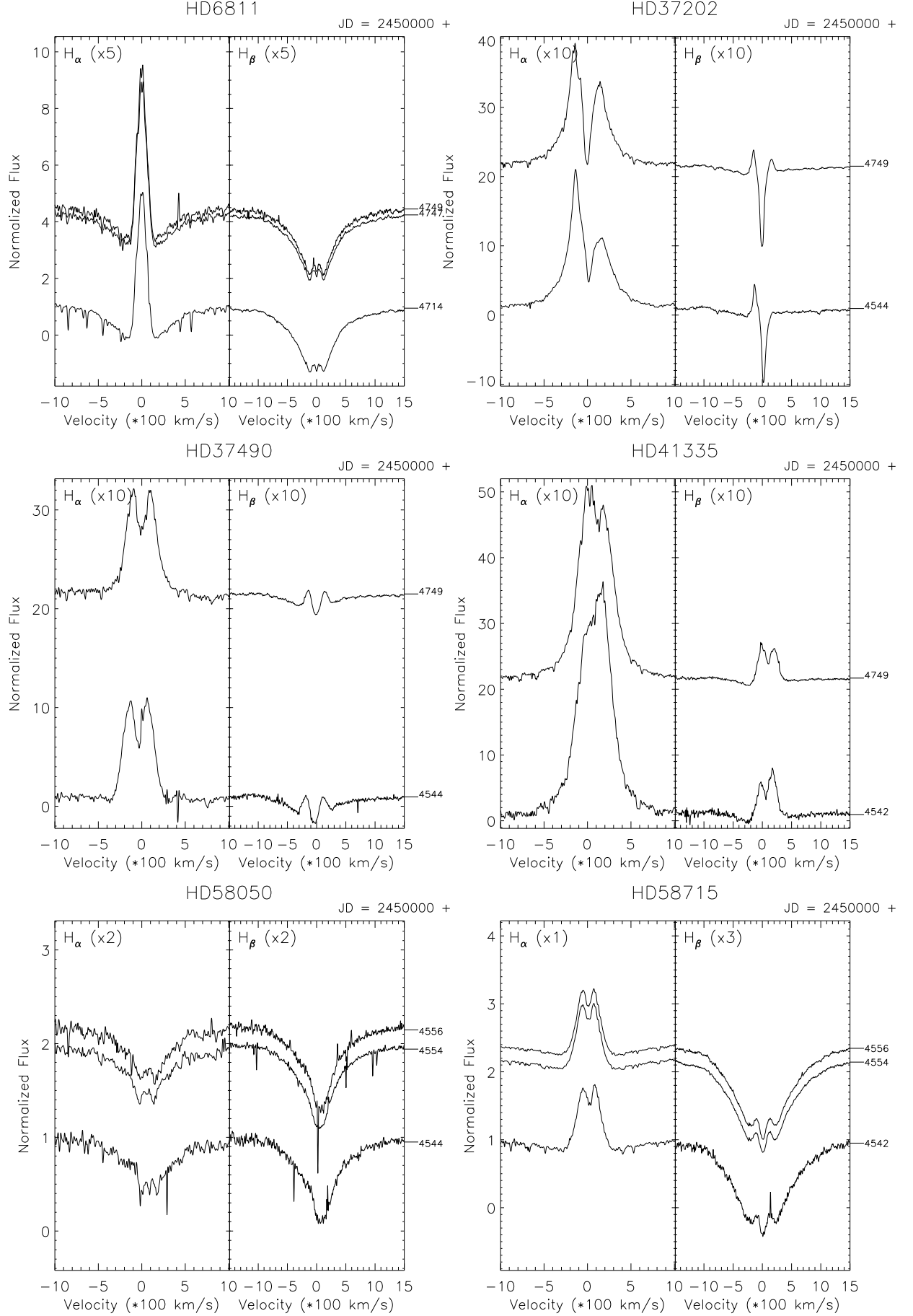


Fig. B.1. Line profiles of $H\alpha$ and $H\beta$ observed for our program stars. Spectra have been shifted along the vertical axis according to the Julian Day of their observation, whose last four digits are reported. In parenthesis we report the magnification factors applied to each profiles in order to improve the visualization.

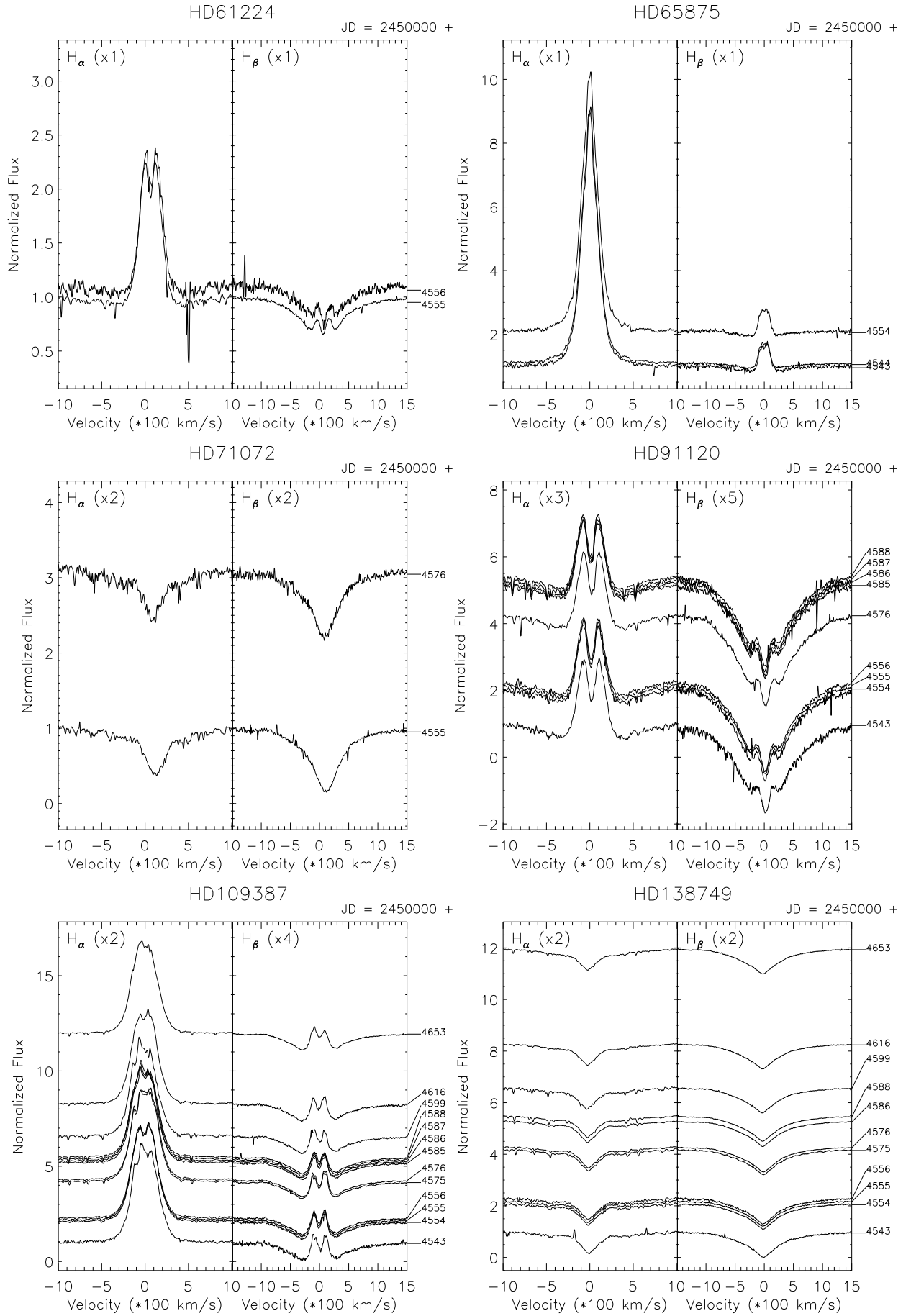


Fig. B.2. As in Fig. B.1

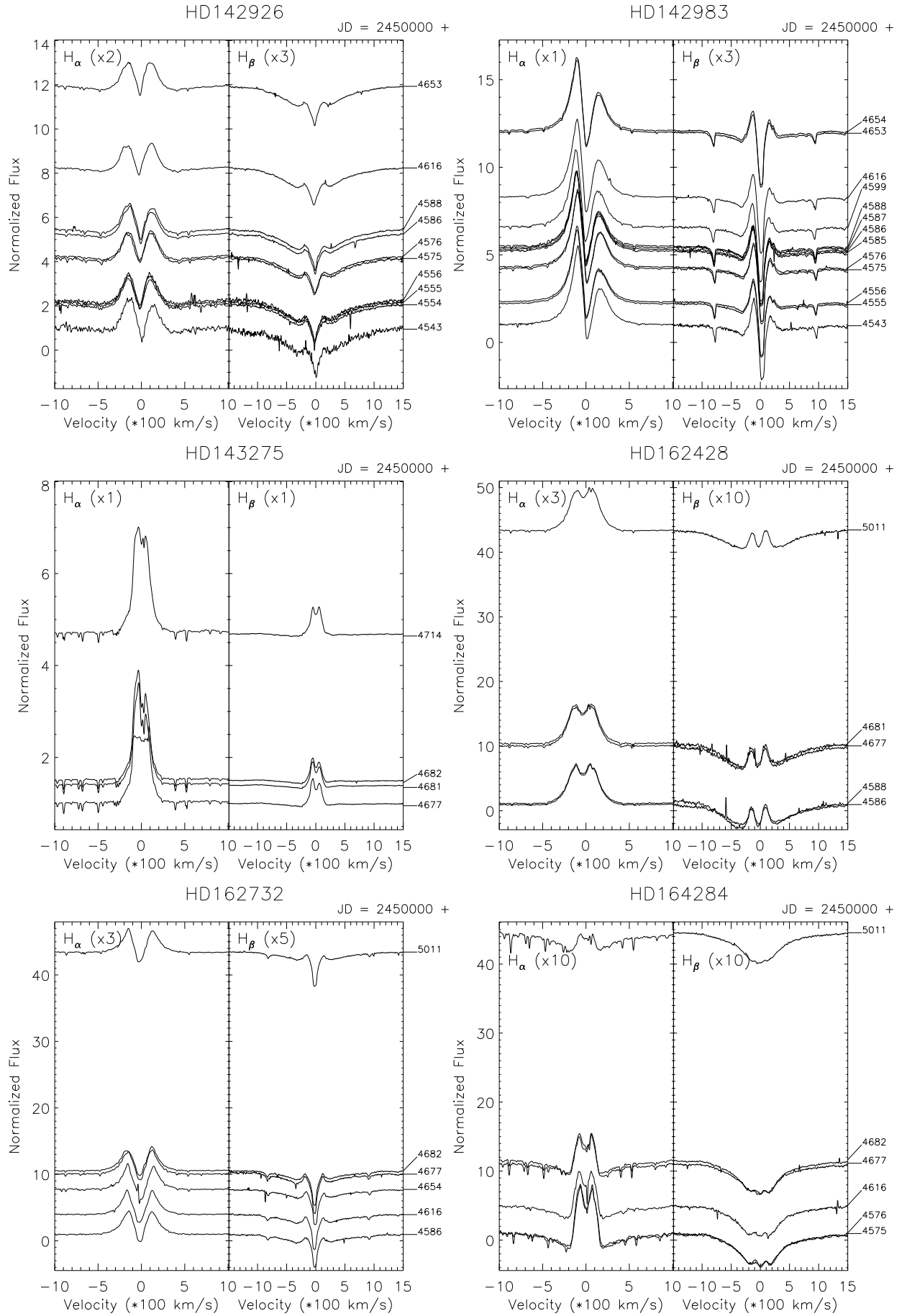


Fig. B.3. As in Fig. B.1

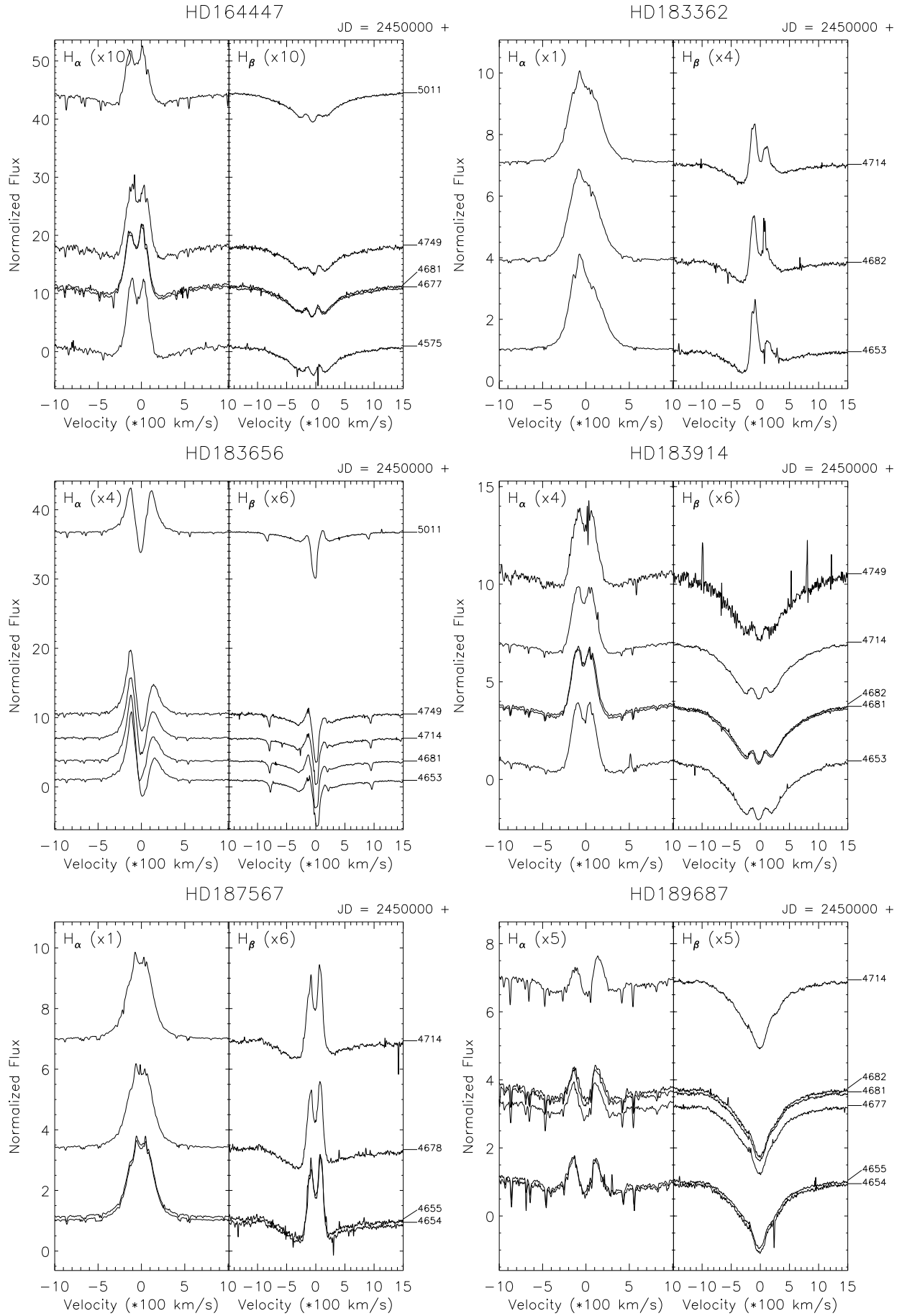


Fig. B.4. As in Fig. B.1

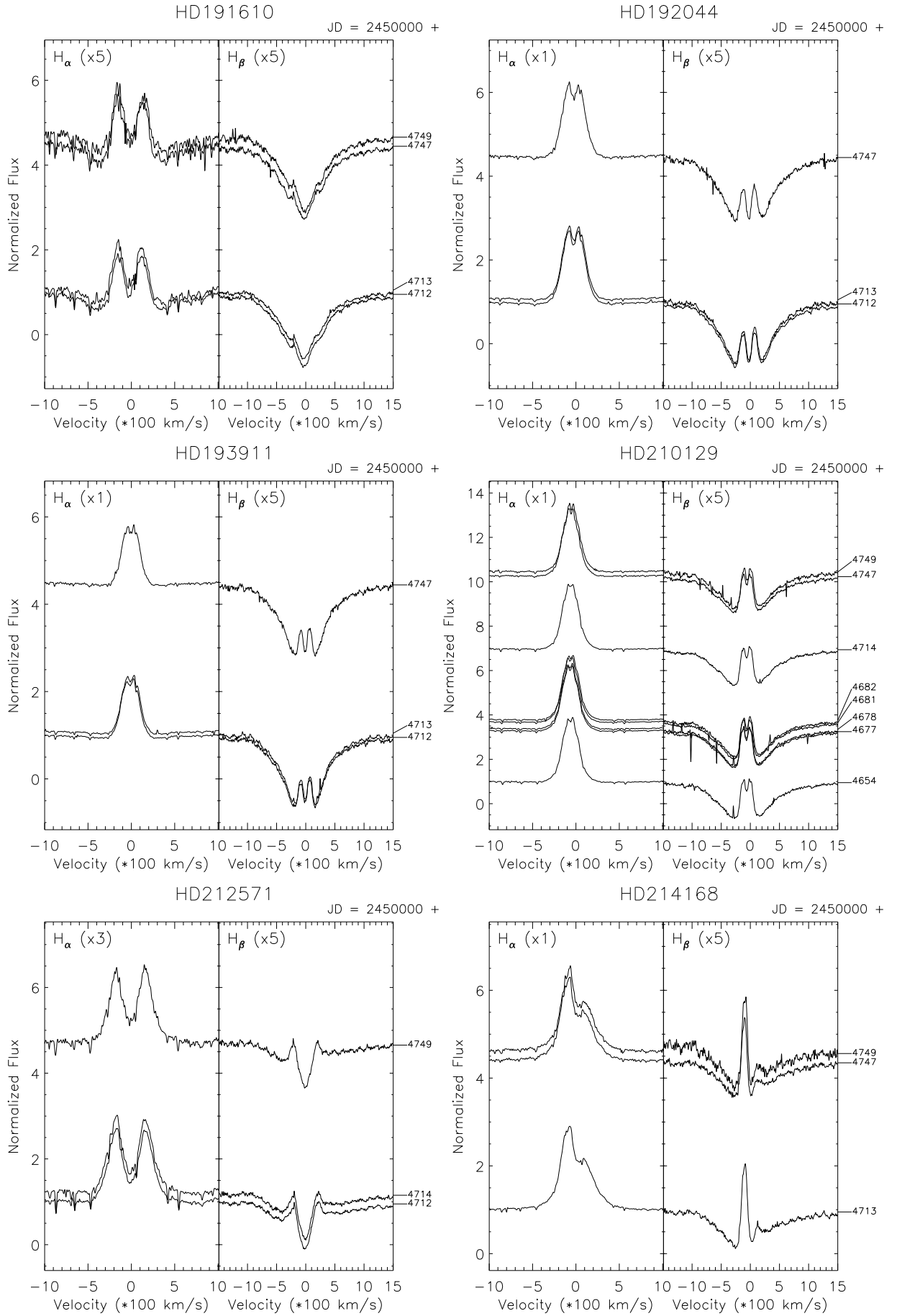


Fig. B.5. As in Fig. B.1

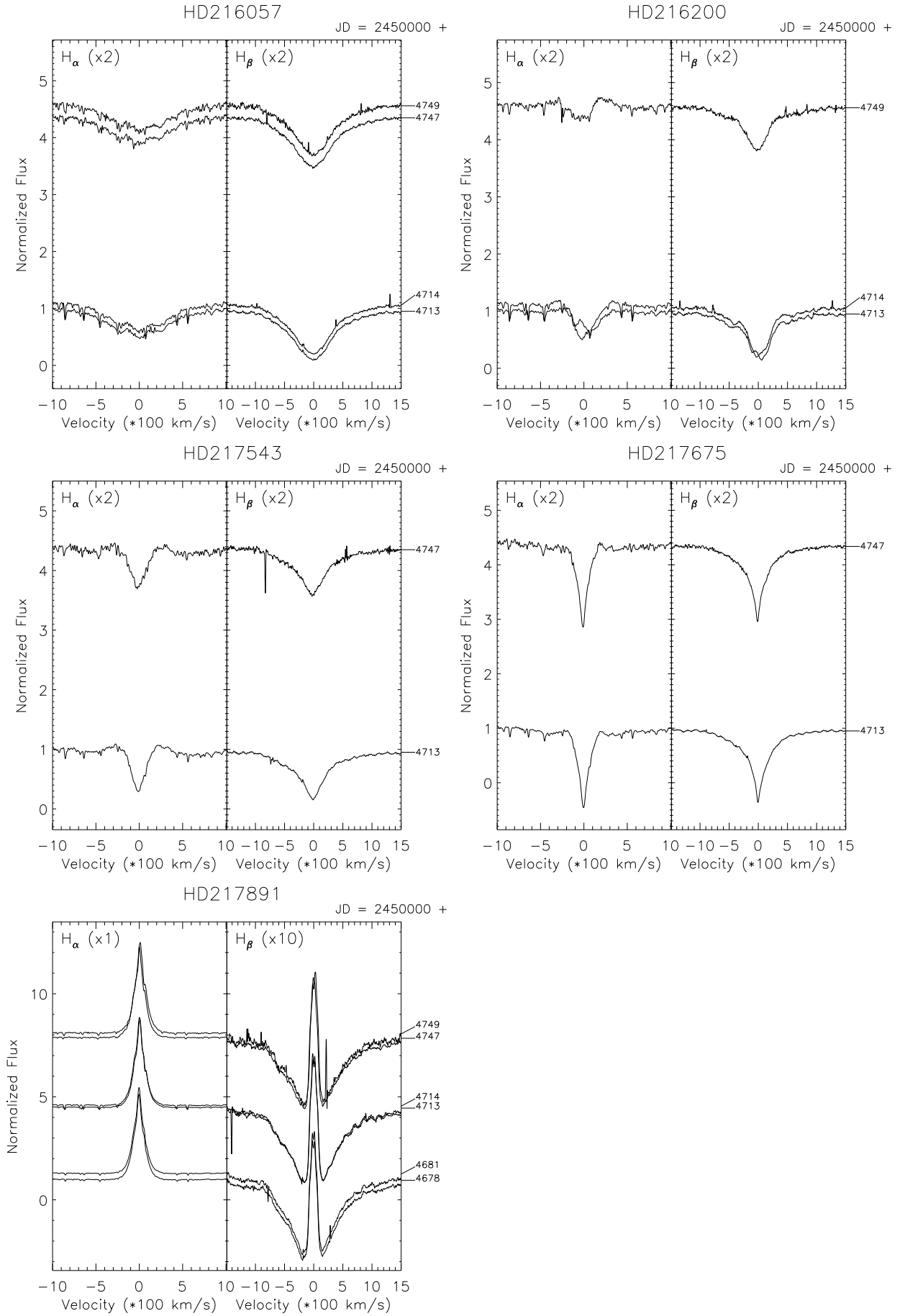


Fig. B.6. As in Fig. B.1

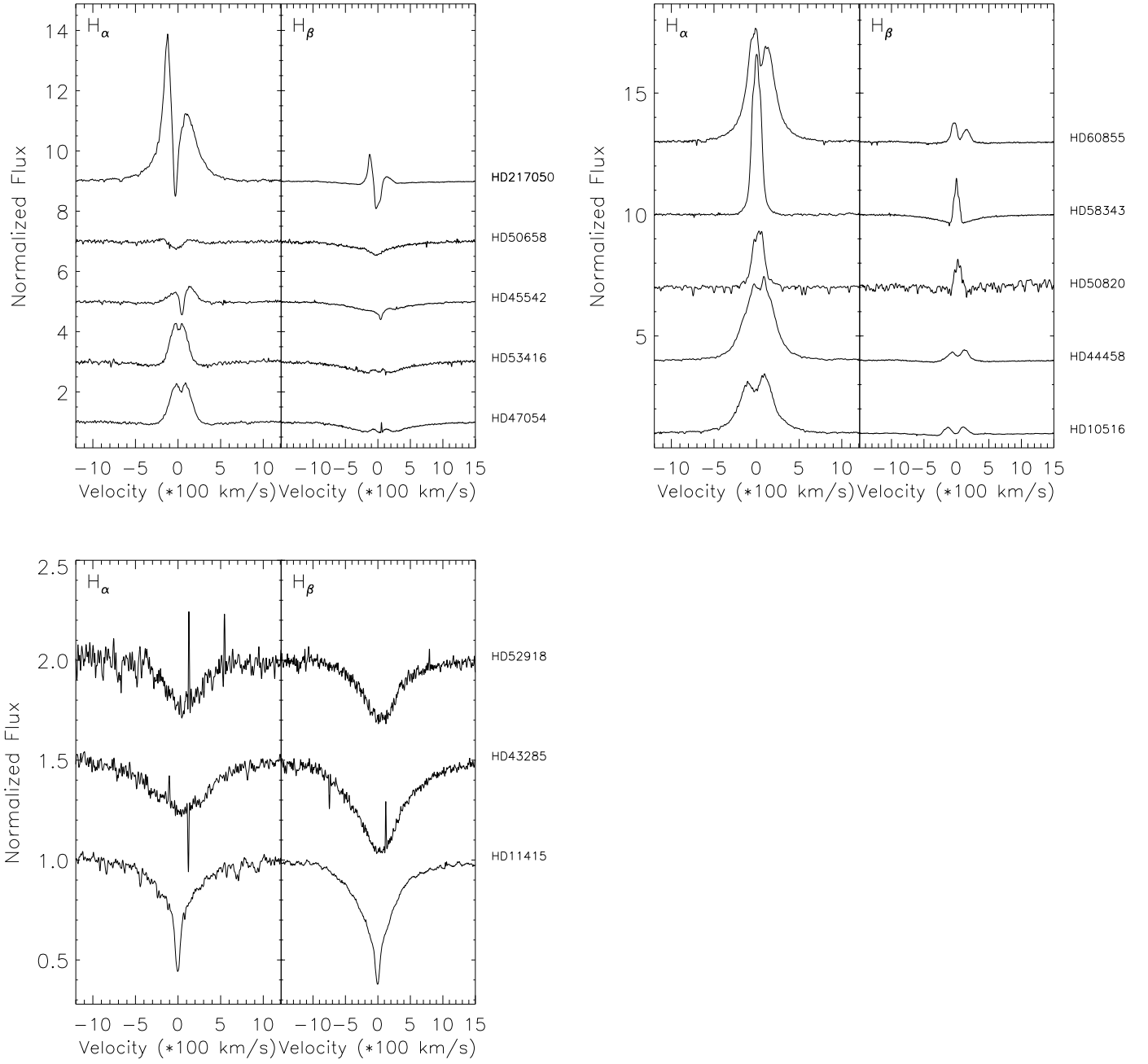


Fig. B.7. $H\alpha$ and $H\beta$ profile for stars for which we only have one spectrum. In the boxes we display shell and class 1 stars, class 2 stars, and stars showing absorption, respectively.